

Direct effects of the environment on AGN triggering in SDSS spiral galaxies: merger-AGN connection

Minbae Kim,^{1*} Yun-Young Choi,^{1,2†} and Sungsoo S. Kim^{1,2}

¹*School of Space Research, Kyung Hee University, Yongin, Gyeonggi 17104, Republic of Korea*

²*Department of Astronomy & Space Science, Kyung Hee University, Yongin, Gyeonggi 17104, Republic of Korea*

Accepted XXX. Received YYY; in original form ZZZ

ABSTRACT

We examine whether galaxy environments directly affect triggering nuclear activity in Sloan Digital Sky Survey (SDSS) local spiral galaxies using a volume-limited sample with the r -band absolute magnitude $M_r < -19.0$ and $0.02 < z < 0.055$ selected from the SDSS Data Release 7. To avoid incompleteness of the central velocity dispersion σ of the volume-limited sample and to fix the black hole mass affecting AGN activity, we limit the sample to a narrow σ range of $130 \text{ km s}^{-1} < \sigma < 200 \text{ km s}^{-1}$. We define a variety of environments as a combination of neighbour interactions and local density on a galaxy. After the central star formation rate (which is closely related to AGN activity level) is additionally restricted, the direct impact of the environment is unveiled. In the outskirts of rich clusters, red spiral galaxies show a significant excess of the AGN fraction despite the lack of central gas. We argue that they have been pre-processed before entering the rich clusters, and due to mergers or strong encounters in the in-fall region, their remaining gases efficiently lose angular momentum. We investigate an environment in which many star-forming galaxies coexist with a few starburst-AGN composite hosts having the highest [OIII] luminosity. We claim that they are a gas-rich merger product in groups or are group galaxies in-falling into clusters, indicating that many AGN signatures may be obscured following the merger events.

Key words: galaxies: active - galaxies: evolution - galaxies: formation - galaxies: interactions - galaxies:spiral - galaxies: clusters: general

1 INTRODUCTION

It is generally accepted that the active galactic nuclei (AGNs) are powered by feeding supermassive black holes (SMBHs) via matter accretion at a galactic central region (Lynden-Bell 1969; Rees 1984). AGN activity depends primarily on the availability of cold gas fuel and the BH mass of their host galaxies, which are closely related to the properties of the host galaxy (Moles et al. 1995; Choi et al. 2009; Schawinski et al. 2010; Sabater et al. 2012, 2015; Argudo-Fernández et al. 2018), as well as to the gas transporting mechanisms to the galactic central region near the SMBHs. Possible SMBHs feeding gas inflow mechanisms include internal dynamical processes such as bar-driven gas inflow (Shlosman et al. 1990; Combes 2003; Kormendy & Kennicutt 2004), turbulence in interstellar matter (Elmegreen et al. 1998; Wada 2004; Wada et al. 2009) and stellar wind (Ciotti & Ostriker 2007; Davies et al. 2012), as well as the external processes

such as galaxy interactions and mergers (Sanders et al. 1988; Hernquist & Mihos 1995; Di Matteo et al. 2005; Springel et al. 2005; Hopkins et al. 2006; Alonso et al. 2007; Haan et al. 2009).

Due to the very large data sets of galaxies provided by Sloan Digital Sky Survey (SDSS), statistically significant studies on the possible link between AGN activity and the environments of host galaxies have become possible. Several studies have determined the correlation between galaxy interactions and AGN activity (Ellison et al. 2011; Hwang et al. 2012; Liu et al. 2012; Satyapal et al. 2014; Weston et al. 2017; Goulding et al. 2018). For example, Ellison et al. (2011) and Satyapal et al. (2014) found that the AGN fraction increases at small projected separations using SDSS galaxy samples of close pairs. Hwang et al. (2012) found that the environmental dependence of the AGN fraction varies with the host galaxy morphology. Liu et al. (2012) also found that both AGN activity and recent star formation of host galaxies increase when pair separation decreases in AGN pair samples. Observations have also shown the role of the local density environment in AGN activity. von der Linden et al. (2010) found that the AGN fraction

* E-mail: mbkim@khu.ac.kr

† E-mail: yy.choi@khu.ac.kr

of quiescent red galaxies in SDSS cluster galaxy samples decreases towards the centre of the clusters. Sabater et al. (2013) showed that the AGN fraction decreases towards denser environments using a density estimator defined using the distance to the 10th nearest neighbour.

However, some observational studies have found contradictory results (Grogin et al. 2005; Darg et al. 2010; Slavcheva-Mihova & Mihov 2011; Scott & Kaviraj 2014; Villforth et al. 2014). Darg et al. (2010) found no significant differences in the environmental distributions of merger samples and randomly selected control samples from SDSS and Galaxy Zoo samples. Slavcheva-Mihova & Mihov (2011) showed that Seyfert nuclei triggering is not directly related to the large-scale morphology or local environment of their host galaxies, including bars, rings and close companions. Grogin et al. (2005) showed that symmetry parameter of AGN hosts is not different from that of non-AGN hosts, suggesting that there is no relation between galaxy interaction and AGN activity.

On the other hand, when the morphology of their host galaxies is fixed, more interesting results have been revealed. Using the SDSS cluster galaxy sample, Hwang et al. (2012) investigated environmental effects on AGN activity by comparing galaxies in the cluster and field. For spiral galaxies, the AGN fraction does not change much, beginning to decrease only near the cluster centre. Elliptical galaxies in cluster have obviously lower AGN fractions than those in the field. Sohn et al. (2013) also found similar results where the AGN fractions for elliptical galaxies significantly decrease with increasing galaxy number density, whereas the fractions for spiral galaxies change very little, even in compact groups where galaxies may experience frequent galaxy interactions. Alonso et al. (2013) found that for face-on spiral AGN host galaxies, the powerful AGN fraction increases in denser environments using a projected local density parameter defined by the fifth nearest neighbour. Argudo-Fernández et al. (2016) found the environmental effects are different depending on the stellar mass of the galaxy. The AGN fractions of very massive and isolated galaxies increase when transitioning from void to denser environment regions, whereas those of galaxies with low-mass decrease.

Here, a question arises about the direct and indirect effects of the external factors on the AGN triggering. The external factors effectively control the gas supply to galaxies, but it is not clear whether they directly or indirectly affect AGN activity in the innermost part of a galaxy. Therefore, when investigating the direct connection between AGN activity and galaxy environment, which we aim to do in this work, galaxy properties closely related to gas availability need to be fixed.

Motivated by this, we select ‘bulge-dominated’ spiral galaxies that more dominantly host AGNs and are located across more diverse environments, ranging from void to cluster environments. To examine the direct environmental impact, we additionally fix a central star formation (SF) because AGN activity is better linked to the central SF than to galaxy-wide SF or $u - r$ colour (Kauffmann et al. 2007; LaMassa et al. 2013; Kim et al. 2019). We use a fibre star formation rate, SFR_{fib} as a proxy of the central SF. To ensure that the diameter (3 arcsec) of the SDSS optical fibre covers the inner few kpc of the sample galaxy, we fix the red-

shift upper limit of the SDSS volume-limited sample to be $z = 0.055$. At the median redshift of our sample ($z = 0.043$), the fibre subtends to ~ 2.7 kpc, which is similar to the average size of bulges in spiral galaxies (Fisher & Drory 2010; Cheung et al. 2015). As a result, the SFR_{fib} s in our sample well represent more confined central activity.

Our sample selection and definitions of the environments are described in Section 2. For each target galaxy, we measure two different environmental parameters: level of galaxy–galaxy interaction (the projected separation of the nearest pair galaxy from the target galaxy, r_p) and large-scale environment (the background density described by the 20 closest galaxies, ρ_{20}). In Section 3, we investigate their combined effects on the triggering of AGN. We additionally limit the central SFR_{fib} of the sample to isolate the effect on only AGN activity. Our discussion and summary are presented in Sections 4 and 5. Throughout this paper, the cosmological parameters are assumed for the Λ CDM cosmological model with the density parameters $\Omega_m = 0.27$ and $\Omega_\Lambda = 0.73$.

2 OBSERVATIONAL DATA SAMPLE

2.1 Sloan Digital Sky Survey

We select a volume-limited spiral-galaxy sample with an r -band absolute magnitude $M_r < -19.5 + 5\log h$ (hereafter we exclude the $+5\log h$ term in the absolute magnitude term) and redshift $0.02 < z < 0.055$ from Sloan Digital Sky Survey Data Release 7 (SDSS DR7; Abazajian et al. 2009). We also use several Value-Added Galaxy Catalogues (VAGCs) for SDSS DR7 for the physical parameters of the host galaxies.

For the fibre and total star formation rates (SFR_{fib} and SFR_{tot} respectively) and the information of optical emission lines of late-type galaxies in our sample, we adopt spectroscopic parameters from the Max Planck Institute for Astrophysics and Johns Hopkins University (MPA/JHU) DR8 catalogue. For calculating the SFR_{fib} of star-forming galaxies (SFGs), emission lines were used (Brinchmann et al. 2004), while those for the others types were calculated using fibre photometry (Salim et al. 2007). We adopt photometry parameters such as M_r , $u - r$ colour, $\Delta(g - i)$, and c_{in} from the Korea Institute for Advanced Study DR7 Value-Added Galaxy Catalogue (KIAS DR7-VAGC; Park & Choi 2005; Choi et al. 2010), which is complementary to the New York University Value-Added Galaxy Catalogue (NYU VAGC; Blanton et al. 2005) and MPA/JHU catalogue.

The stellar velocity dispersion σ is a good indicator of BH mass ($M_{\text{BH}} \propto \sigma$ relation; Ferrarese & Merritt 2000; Gebhardt et al. 2000; Tremaine et al. 2002; Gültekin et al. 2009; Batista et al. 2017). We set 70 km s^{-1} as a lower limit on σ measurements due to the instrumental resolution of the SDSS spectrograph. The σ measurements adopted from NYU-VAGC are used only for spectra with median signal-to-noise (S/N) per pixel > 10 and are corrected for the aperture of an SDSS spectroscopic fibre (Bernardi et al. 2003).

2.2 Morphology classification

Morphology classification is adopted from the KIAS DR7-VAGC. The galaxy morphology is divided into early-type

Table 1. Spectral type classification statistics and comparison of results with different emission line S/N cuts

Number (Fraction)	S/N ≥ 6	S/N ≥ 3
Total ($\sigma > 70 \text{ km s}^{-1}$)	11 096 (1.00)	11 096 (1.00)
SFG	3451 (0.31)	4743 (0.43)
Total AGN	2942 (0.27)	3973 (0.36)
Composite	2209 (0.20)	3153 (0.28)
Pure AGN	733 (0.07)	820 (0.07)

(ellipticals and lenticulars) and late-type (spirals and irregulars) based on their locations in two parameter space (Park & Choi 2005): $u-r$ colour versus $g-i$ colour gradient ($\Delta(g-i)$) space and $u-r$ colour versus i -band concentration index (c_{in}) space. $\Delta(g-i)$ is the difference in $g-i$ colours between the outside $0.5R_{\text{Pet}} < R < R_{\text{Pet}}$ and the inside in $R < 0.5R_{\text{Pet}}$ of the galaxy, where R_{Pet} is the Petrosian radius in the i -band. If $\Delta(g-i)$ is positive/negative, this means there is a bluer/redder core and redder/bluer outside. The c_{in} is defined as the ratio of R_{50} and R_{90} which are the Petrosian radii with fluxes of 50% and 90% smaller in the i -band. Commonly, the c_{in} of an early-type galaxy is smaller than that of a late-type galaxy. We use 11 096 late-type galaxies with $\sigma > 70 \text{ km s}^{-1}$ for this study.

2.3 AGN selection

We classify the types of galaxies based on Baldwin-Phillips-Terlevich (BPT) diagrams (Baldwin et al. 1981; Veilleux & Osterbrock 1987). For $H\alpha$, $H\beta$, [OIII] $\lambda 5007$, [NII] $\lambda 6584$ as measured in the MPA/JHU Catalogue (cf. Brinchmann et al. 2004), several flux ratios of narrow emission lines with S/N ≥ 6 are used. Galaxies can be classified as SFGs, starburst-AGN composite galaxies, and pure AGNs (Seyfert and low-ionization nuclear emission-line regions, LINERs). Composite galaxies are located between the maximum starburst line (Kewley et al. 2001) and the pure star-forming line (Kauffmann et al. 2003).

In this study, we define AGNs as Type II AGNs including composite galaxies and pure AGNs using the criterion of Kewley et al. (2006). In our AGN sample, we exclude potential Type I AGNs, which have a full width at half-maximum (FWHM) of an $H\alpha$ emission line larger than $\sim 500 \text{ km s}^{-1}$. Here, one should note that all the LINERs identified by BPT diagram are not bona fide AGNs, some of the weak LINERs are retired galaxies powered by hot low-mass evolved stars rather than low-luminosity AGNs (Stasińska et al. 2008; Cid Fernandes et al. 2010, 2011; Melnick & De Propriis 2013). By adopting the criterion of Cid Fernandes et al. (2011), we exclude LINERs and pure AGNs classified as ambiguous with $W_{H\alpha} < 3$. The result of the spectral type classification is listed in Table 1. Out of 11 096 spiral galaxies with $\sigma > 70 \text{ km s}^{-1}$, 2942 AGN hosts are found.

We conservatively select AGNs using a signal-to-noise ratio of S/N ≥ 6 instead of the commonly used S/N ≥ 3 . Table 1 also shows how the galaxy number of each spectral type varies depending on the signal-to-noise. Unlike SFGs and composite galaxies, which drastically decrease, no sig-

nificant change is found in the number of pure AGNs without retired galaxies. We confirm that the overall results do not change much when S/N ≥ 3 is used instead of S/N ≥ 6 in the definition of an AGN.

2.4 Environmental parameters

To understand the environmental dependence of AGN fraction, two different environmental factors are considered in this study. One is a large-scale background density ρ_{20} defined by the 20 closest galaxies of a target galaxy in the sample. It is just over a few Mpc in scale (see section 2.5 of Park & Choi 2009, for details). The other is the distance between a target galaxy and the pair galaxy. To define the estimates, we use a volume-limited galaxy sample with the r -band absolute magnitude $M_r < -19.0$ and $0.02 < z < 0.055$. The full detail of the estimation for methods $\rho_{20}/\bar{\rho}$ and $r_p/r_{\text{vir,nei}}$ are described in Park et al. (2008) and Park & Choi (2009).

2.4.1 Large-scale background density

The large-scale background density of a target galaxy is given by

$$\rho_{20}(\mathbf{x})/\bar{\rho} = \sum_{i=1}^{20} \gamma_i L_i W_i(|\mathbf{x}_i - \mathbf{x}|)/\bar{\rho}, \quad (1)$$

where the γ_i is the mass-to-light ratio of a background galaxy which is adopted to obtain the mass density described by 20 neighbouring galaxies. Here, the ratio of dark halo virial mass for early- and late-type targets, $\gamma(\text{early}) = 2\gamma(\text{late})$ is only needed. Park & Choi (2009) derived the ratio from the velocity dispersion of neighbouring galaxies around a target and a relation between the velocity dispersion and the virial halo mass of $M_{\text{vir}} \propto \sigma_{\Delta v}^{\beta}$, where $\beta = 2.5$. The mass is related to the galaxy plus dark halo system. The mean density of the Universe with total volume V is obtained by $\bar{\rho} = \sum_{\text{all}} \gamma_i L_i / V$, and $W_i(\mathbf{x})$ and L_i are a smoothing weight function and the r -band luminosity of the closest 20 background galaxies of a target spiral galaxy respectively.

For estimating the large-scale background density, we adopt the spline-kernel weight $W(r)$ as the smooth weight function (Monaghan & Lattanzio 1985). According to Park et al. (2007), the adaptive smoothing kernel better preserves a property of the galaxy distribution than a kernel with a fixed smoothing length and has the advantage that the S/N for estimating density is more uniform. Park et al. (2008) showed that the 20 galaxies required within the adaptive smoothing volume is close to the smallest number yielding good local density estimates.

2.4.2 The nearest neighbour galaxy

The pair galaxy for a host galaxy is defined using the conditions of r -band absolute magnitude and radial velocity difference as that which is located closest to the target galaxy in the sky. If a host galaxy has the r -band absolute magnitude M_r , the nearest neighbour galaxy for that host galaxy has an r -band absolute magnitude brighter than $M_r + \Delta M_r$ and a radial velocity difference less than Δv , making it the most influential neighbour. We adopted $\Delta M_r = 0.5$ and $\Delta v = 400 \text{ km s}^{-1}$

obtained by measuring the pairwise velocity difference between target galaxies and their neighbours (see section 2.4 of [Park et al. 2008](#)).

The pair separation of r_p measures the impact of interactions with the most influential neighbour. The virial radius of the nearest neighbour (i.e., pair galaxy) $r_{\text{vir,nei}}$ is defined as r_p , where the mean mass density ρ_n within the sphere with radius of r_p is equal to 740 times the mean density of the Universe $\bar{\rho}$:

$$r_{\text{vir,nei}} = (3\gamma_{\text{nei}}L_{\text{nei}}/4\pi\bar{\rho}/740)^{1/3}, \quad (2)$$

where γ_{nei} and L_{nei} are the mass-to-light ratio and the r -band luminosity of the nearest neighbour galaxy, respectively. According to this formulae, the virial radii of spiral galaxies with $M_r = -19.5$ corresponds to 210 h^{-1} kpc.

3 RESULTS

3.1 Strong dependence of AGN fraction on galactic central SF

We begin this study by investigating how AGN activity varies depending on two central quantities: the velocity dispersion σ and central star formation rate SFR_{fib} .

Figure 1 shows the distributions of the AGN fractions in the sample (in the left-hand panel) and of the powerful AGN fractions in all AGN hosts (in the right-hand panel) in the $\text{SFR}_{\text{fib}}-\sigma$ space. Each coloured thick-line contour denotes a constant fraction. A two-dimensional histogram of the number density in each panel is plotted together for all galaxies (in the left-hand panel) and AGN hosts (in the right-hand panel), respectively. Superposed on the 2D histogram plot are the contours of constant number densities enclosing 0.5σ , 1σ and 2σ in that order. All the smoothed distributions that we measure hereafter are obtained using the fixed-size spline kernel for each bin (60 by 60) in the parameter space. The corresponding bin size for the $\text{SFR}_{\text{fib}}-\sigma$ plane is $\Delta(\log \sigma) = 0.013$ by $\Delta(\log \text{SFR}_{\text{fib}}) = 0.090$, and for the environment parameter space of r_p and ρ_{20} , the bin size is $\Delta(\log r_p/r_{\text{vir,nei}}) = 0.080$ by $\Delta(\log \rho_{20}/\bar{\rho}) = 0.080$.

AGN activity is measured by calculating AGN occupation fraction f_{AGN} as a ratio between AGN hosts and all galaxies. Assuming that the [OIII] emission-line luminosity $L_{[\text{OIII}]}$ and σ estimate the BH accretion rate and a BH mass, respectively, we calculate the [OIII] line luminosity normalized by BH mass, which measures how rapidly a BH has grown to its present-epoch mass (i.e., a tracer of AGN power). The powerful AGN fraction is given by a ratio between AGNs with $\log L_{[\text{OIII}]} / M_{\text{BH}} > 0.1$ and all AGNs. The M_{BH} is derived from the $M_{\text{BH}}-\sigma$ relation for galaxies given by [Tremaine et al. \(2002\)](#).

Our sample galaxies show a trimodal number distribution in the $\text{SFR}_{\text{fib}}-\sigma$ space that exhibits three distinct peaks: each peak is dominated by galaxies with three different spectral types, SFGs, AGN hosts, and quiescent galaxies.

At a given σ , AGNs in galaxies with the largest SFR_{fib} s composing of an SFG sequence are rarely found but are the most powerful. f_{AGN} reaches its peak when both the SFR_{fib} (consisting of the SFG fraction, f_{SFG}) and the power of the detected AGN considerably decreases. After the f_{AGN} peak, with decreasing SFR_{fib} , f_{AGN} decreases and the reduced power of AGNs changes very little, i.e., AGNs seem

to fade enough. The strong correlation between AGN luminosity and current SF is clearly revealed when measured over the central region, implying that the SFR_{fib} (central SF activity) and $L_{[\text{OIII}]}$ (BH accretion rate) are linked through the central gas supply. For example, for the population with the highest SFR_{fib} , $L_{[\text{OIII}]}$ of their detected AGNs is also highest, but their f_{AGN} is rather lowest. In other words, f_{AGN} is not directly connected with SFR_{fib} and $L_{[\text{OIII}]}$.

Here we should keep in mind that the AGN fraction we calculated is not the probability of triggering AGN in a galaxy, but rather the probability of detecting the triggered AGN. This is because all triggered AGNs may not be detected on the optical band. That is, a low value of f_{AGN} means that AGN is difficult to trigger or that it is difficult to detect the triggered AGN.

Here, we assume that if a large amount of gas funnels into the galactic centre, it drives starburst and a nuclear gas-inflow and given the high $L_{[\text{OIII}]}$ of the observed AGNs, many AGNs are triggered but obscured by dense gas and dust (see [Hickox & Alexander 2018](#), for a review). During this starburst phase, SMBHs may grow rapidly, raising their σ . The obscured AGNs are hidden in galaxies with higher SFR_{fib} and larger σ that lie slightly above the SFG sequence (e.g., [Chang et al. 2017](#)). After galaxies leave the SFG sequence, many AGNs become suddenly observable at larger σ and lower SFR_{fib} and their luminosity is no longer as luminous as before, implying that this process has taken place quite abruptly.

If so, how are they eventually unobscured? As a main cause of the rapid SF quenching, a strong gas outflow driven by powerful AGNs is usually invoked to eject the surrounding gas and dust (e.g., [Di Matteo et al. 2005](#); [Hopkins et al. 2005](#)). [Ishibashi & Fabian \(2016\)](#) claimed in this picture that AGN feedback and starburst are intrinsically coupled. Accordingly, we argue that the population with the highest SFR_{fib} and the lowest f_{AGN} in our sample favours the evolutionary picture of starburst-AGN connection. Meanwhile, after most AGNs are observed, the current SF depletes only remaining gases and the AGNs fade.

Because of the strong dependence of f_{AGN} on σ and SFR_{fib} , it is not easy to observe whether environments directly affect AGN activity without restricting SFR_{fib} and σ values of a sample. For this purpose, we divide the sample into two according to the SFR_{fib} value of the AGN peak at a given σ . A thin diagonal line in Figure 1 separates the two subsamples. We assume that each subsample has a different AGN mode (e.g. ‘powerful’ and ‘weak’ AGNs).

Next, let us note the strong σ dependence of the AGN fraction. From the right-hand panel of Figure 1, when AGN power is given, the $L_{[\text{OIII}]}$ of AGN hosts with a smaller σ is also lower. For weak AGNs, detection of the [OIII] line in the smaller σ galaxies is more difficult and the weak AGNs can be missed during AGN detection (e.g., [Aird et al. 2012](#)). Furthermore, our sample is missing many galaxies with a smaller σ due to the cut of $M_r < -19.5$ adopted to select our volume-limited samples. Hereafter, to avoid the $L_{[\text{OIII}]}$ -related selection effects and incompleteness at lower σ values, we only use a galaxy sample with $130 \text{ km s}^{-1} < \sigma < 200 \text{ km s}^{-1}$. The BH mass range corresponding to the σ range is $7.4 < \log(M_{\text{BH}}/M_{\odot}) < 8.1$. The median and lower and upper quartile BH masses of this sample are $10^{7.56}$, $10^{7.44}$, and $10^{7.72} M_{\odot}$, respectively.

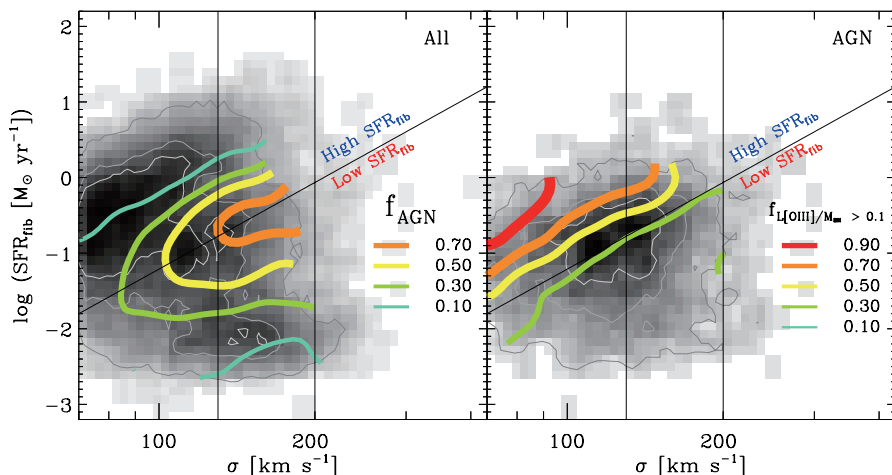


Figure 1. Distributions of the f_{AGN} in the sample galaxies (left) and of the powerful AGN fraction in AGN hosts (right) on the $\text{SFR}_{\text{fib}}-\sigma$ plane. A 2D histogram in each panel shows the number density distribution of galaxies (left) and of AGN hosts (right), respectively. Each grey thin contour for the number density distribution encloses 0.5σ , 1σ and 2σ in that order. For the f_{AGN} distribution, contours with an error greater than 30% of the f_{AGN} measurement are eliminated. The black solid diagonal line divides the sample into two subsamples of high- SFR_{fib} and low- SFR_{fib} samples, which are used in Section 3.3

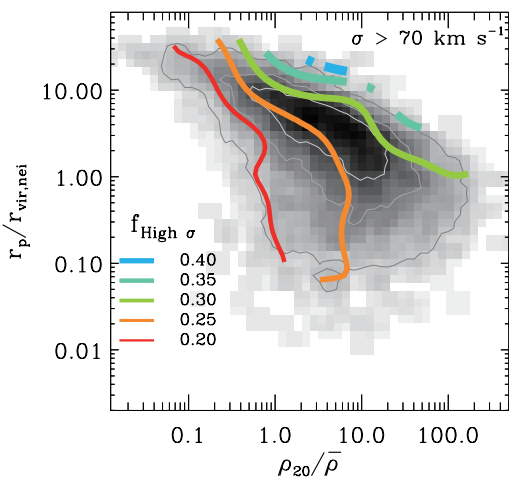


Figure 2. Distribution of the occupation fraction of galaxies with a high σ of $130 \text{ km s}^{-1} < \sigma < 200 \text{ km s}^{-1}$ for our sample in the $r_p-\rho_{20}$ plane. The coloured thick contour line denotes a constant fraction and the contours with an error greater than 30 percent of the fraction measurement are eliminated. The grey 2D histogram represents the number density distributions of the sample and the grey thin contours enclose 0.5σ , 1σ and 2σ of the sample, respectively.

3.2 Environmental dependence of AGN fraction

3.2.1 Galaxy interactions in diverse local environments

First, we limit the sample to a narrow σ range of $130 \text{ km s}^{-1} < \sigma < 200 \text{ km s}^{-1}$. Then, we examine how galaxy interactions and large-scale environments affect AGN activity by measuring the dependence of AGN activity in the r_p and ρ_{20} parameter space. In Figure 2, we show the galaxy number distribution in the $r_p-\rho_{20}$ space measured by using the total sample with $\sigma > 70 \text{ km s}^{-1}$.

In fact, the measurements of the two environmental factors, ρ_{20} and r_p , are entangled by their definitions. The back-

ground density estimate ρ_{20} spans various large-scale environments from voids to clusters. For convenience, we arbitrarily assign the very low density of $\rho_{20} < \bar{\rho}$, intermediate density of $\bar{\rho} < \rho_{20} < 20\bar{\rho}$, and high density of $\rho_{20} > 20\bar{\rho}$ to discrete environmental types such as void/field, group, and cluster environments, respectively. Here, recall that the background galaxies used to define the ρ_{20} are luminous ($M_r < -19.0$). Meanwhile, the pair separation of r_p measures the impact of interactions with the most influential neighbour. According to Park & Choi (2009), when a galaxy approaches the virial radius of its neighbour ($r_p < r_{\text{vir,nei}}$), the two galaxies interact hydrodynamically, which is enough to change the mean morphology and SF activity of the target galaxies (e.g., Park & Choi 2009). When r_p decreases to about 0.05 times $r_{\text{vir,nei}}$ (corresponding to $10 \sim 20 h^{-1} \text{ kpc}$ for our sample), the target and neighbour galaxies start to make physical contact with each other. At some point, the interacting galaxies eventually merge so that the second closest neighbour becomes the nearest neighbour, and consequently, the end-product of the merger is more likely to be located at the largest r_p .

It should be noted that galaxies with $r_p > r_{\text{vir,nei}}$ possess no influential neighbour nearby but can be surrounded by less luminous background galaxies than the nearest neighbour. We consider that among these, galaxies at $\rho_{20} < \bar{\rho}$ where there exist few interacting pairs with $r_p > r_{\text{vir,nei}}$ are in a field environment that do not belong to any galaxy group or cluster. These galaxies can be used as a control for understanding the effects of galaxy interactions and mergers in this study.

The $r_p-\rho_{20}$ diagram shows how these two parameters are intricately related. At $r_p > r_{\text{vir,nei}}$, the r_p and ρ_{20} are largely closely correlated, but at smaller pair separations below $r_p \sim 0.5 r_{\text{vir,nei}}$, the correlation tends to disappear. Accordingly, the intermediate background density surrounding a target galaxy provides the widest r_p distribution. In other words, the $r_p-\rho_{20}$ diagram demonstrates that a sin-

gle measurement of r_p or ρ_{20} cannot properly describe the environment in which a galaxy resides.

Each coloured thick contour in Figure 2 denotes a constant fraction of galaxies having $130 \text{ km s}^{-1} < \sigma < 200 \text{ km s}^{-1}$. The contours show the σ distribution over the r_p – ρ_{20} space. At the largest r_p s in the intermediate- ρ_{20} region, the highest occupation fraction of the high- σ galaxies is found, suggesting that mergers contribute significantly to bulge growth. The location provides a suitable environment for observing the merger-AGN connection that SMBH-galaxy co-evolution is driven by galaxy mergers (e.g., Di Matteo et al. 2005; Hopkins et al. 2008; Alexander & Hickox 2012; Treister et al. 2012).

Given the relatively low velocities of group galaxies (about 50 to 400 km s^{-1} , McCannachie et al. 2009), mergers and galaxy interactions are expected to be more frequent in group environments than in cluster environments, so the intermediate-density region at $r_p < r_{\text{vir,nei}}$ roughly corresponds to a group environment. Figure 3 below confirms that cluster member galaxies are mainly found in higher density region than roughly $\rho_{20} \sim 20\bar{\rho}$ where more galaxies are gravitationally bound. The inner first and second grey contours in Figure 2 include about 38% and 68% of the sample, respectively. Out of the sample, 17.5% has a small pair separation of $r_p < r_{\text{vir,nei}}$ and belongs to groups or clusters.

To check where cluster member galaxies are actually distributed in the r_p and ρ_{20} space, we plot Figure 3. By using the SDSS DR9 galaxy clusters catalogue of Banerjee et al. (2018), we found 68 galaxy clusters (with cluster richness $\Lambda_{200} > 20$) at $0.045 \leq z < 0.055$ overlapping the redshift range of our sample. Only 15 clusters located within the survey region of our sample were finally selected. Clusters sitting close to the survey boundaries were also excluded.

Based on the simulation result by Serra & Diaferio (2013), we identified 131 spiral galaxies as cluster member galaxies from the galaxy sample with $0.042 \leq z < 0.055$ and $\sigma > 70 \text{ km s}^{-1}$. Galaxies having a line-of-sight velocity difference from the clusters below 1000 km s^{-1} within clustercentric radii of $2r_{200,\text{cl}}$ were conservatively selected. The $r_{200,\text{cl}}$ is the radius of the sphere whose mean overdensity drops to 200 times the critical density of the universe. The mean $r_{200,\text{cl}}$ of the 15 clusters is about 1 Mpc. Out of 131 galaxies, 73 galaxies at $r_{\text{ctr}} < r_{200,\text{cl}}$ and 58 galaxies at $r_{\text{ctr}} = 1 \sim 2r_{200,\text{cl}}$ were considered to be in the cluster virial and in-fall regions, respectively. The orange and blue contours represent the number density distributions of the galaxies with $r_{\text{ctr}} < r_{200,\text{cl}}$ and $r_{\text{ctr}} = 1 \sim 2r_{200,\text{cl}}$, respectively. The 2D histogram represents the number density distribution of the galaxy sample selected for this test. The contours for each sample enclose 0.5σ and 1σ .

Figure 3 shows that the identified cluster member galaxies mostly locate in the high-density region of $\rho_{20} > 10\bar{\rho}$. For convenience, in this study, we define the region of $\rho_{20} > 20\bar{\rho}$ as a cluster environment. Compared to the cluster galaxies in the cluster virial region, galaxies in the cluster outskirts locate at relatively larger $r_p = 1 \sim 2r_{\text{vir,nei}}$. When galaxies have smaller r_p and larger ρ_{20} , they are more likely to locate at smaller clustercentric distances.

It can be seen that at smaller r_p s in the region of $\rho_{20} > 20\bar{\rho}$, spiral galaxies suddenly disappear, which is a natural consequence, given the morphology–density rela-

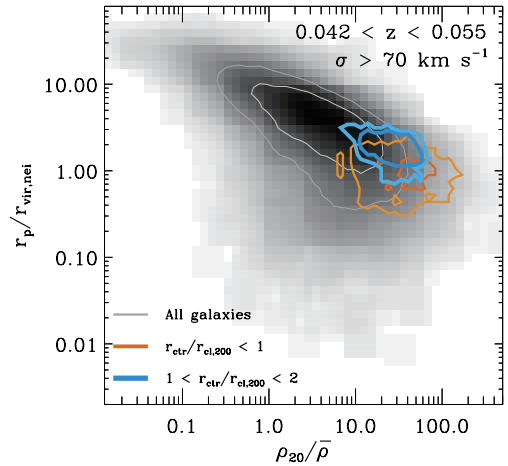


Figure 3. Distribution of cluster member galaxies in the galaxy sample with $0.042 \leq z < 0.055$ and $\sigma > 70 \text{ km s}^{-1}$. The number distribution of the whole sample is represented by the grey 2D histogram and grey thin contours. The orange and blue thin contours show the number density distributions of galaxies within cluster virial radius of $r_{\text{ctr}} < r_{200,\text{cl}}$ and galaxies in the cluster outskirts of $r_{\text{ctr}} = 1 \sim 2r_{200,\text{cl}}$, respectively. The thin contours enclose 0.5σ and 1σ of each sample, respectively.

tion. That is, the smaller r_p region where the spiral galaxies disappear corresponds to the inner region of clusters where the elliptical galaxy is preferentially located. In this context, given that more spiral galaxies are found in poor clusters (or groups) and often in their inner regions, we can infer that many of galaxies with $r_p < 0.5r_{\text{vir,nei}}$ in a cluster environment may be members located in the inner region of poor clusters.

According to the hierarchical structure formation paradigm, as ρ_{20} increases, galaxies join more and more rich and massive systems. The region of $\rho_{20} > 50\bar{\rho}$ may contain many rich clusters. The cluster catalogue we used seems to be missing many poor clusters. Hwang et al. (2012) resolved the virialized cluster regions using the SDSS Abell clusters data and studied AGN activity dependence of galaxies within $10r_{200,\text{cl}}$ on the r_{ctr} and r_p .

We conclude that in order to adequately describe the environment of a galaxy, one should consider the combined effect of the two r_p and ρ_{20} .

3.2.2 Environmental dependence of AGN fraction in spirals with a high σ

In Section 3.1, we have shown that AGN triggering primarily correlates with SFR_{fib} and σ of galaxies. In this section, by fixing those most influential properties, we investigate the direct impact of the environment on AGN triggering. First, we measure the impact for the σ -limited sample, seen in the left and middle panels of Figure 4. To check the statistical significance of the several features found from Figure 4, we plot Figure 5.

At a given r_p , SFR_{fib} increases with decreasing ρ_{20} . When $r_p < r_{\text{vir,nei}}$, the ρ_{20} dependence of SFR_{fib} becomes obvious. The highest SFR_{fib} enhancement is found in group galaxies with $r_p < 0.3r_{\text{vir,nei}}$, implying that the neighbour interaction in groups is a dominant process of the central SF enhancement of a host galaxy.

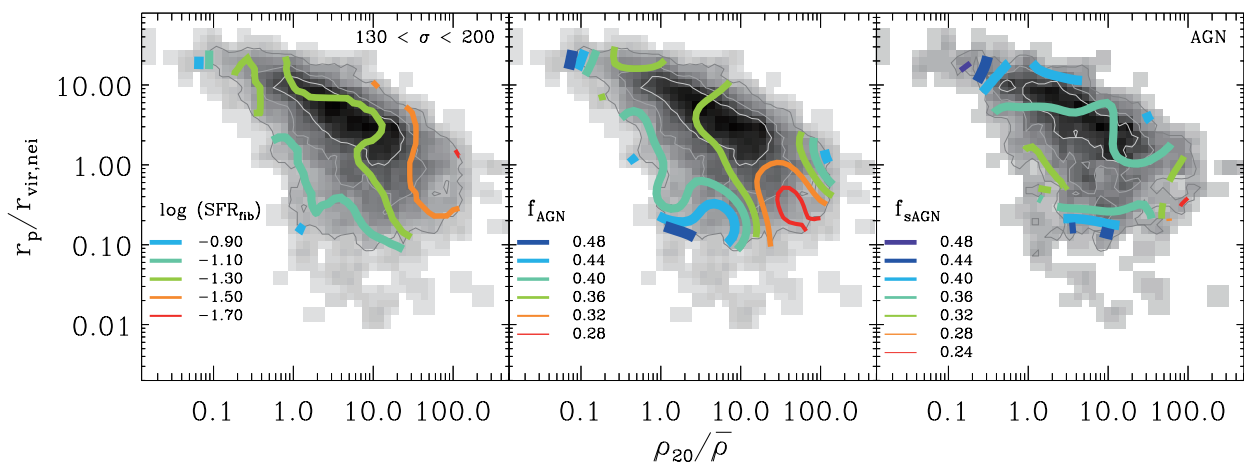


Figure 4. The distributions in the r_p – ρ_{20} plane of $\log(\text{SFR}_{\text{fib}})$ (left) and f_{AGN} (middle) at given σ with $130 \text{ km s}^{-1} < \sigma < 200 \text{ km s}^{-1}$. The right-hand panel shows the distribution of the strong AGN fraction with $\log(L_{[\text{OIII}]} / L_{\odot}) > 6.42$ in AGN host galaxies. The coloured thick contour lines denote each distribution. The grey 2D histograms and thin contours represent the number density distributions of galaxies (left and middle) and AGN hosts (right), respectively. The thin contours enclose 0.5σ and 1σ of each sample, respectively.

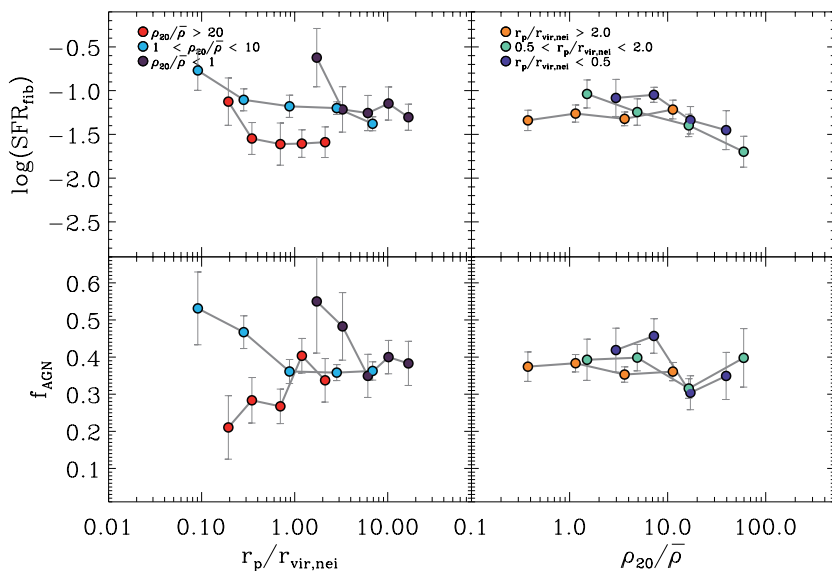


Figure 5. Behaviours of f_{AGN} and SFR_{fib} as a function of r_p at a fixed ρ_{20} (left) and as a function of ρ_{20} at a given r_p (right) for the high- σ sample. The colour of the dots changes depending on ρ_{20} (left) or r_p (right). The errors represent 1σ deviation from 1000 bootstrap resampling.

On the other hand, interacting galaxies with $r_p < r_{\text{vir,nei}}$ also undergo major changes in f_{AGN} . In particular, for group galaxies, the f_{AGN} rapidly increases at $r_p < 0.3r_{\text{vir,nei}}$ where the increase in SFR_{fib} occurs. The luminosity of AGNs found there are brighter than those found elsewhere, as seen from the right-hand panel of Figure 4. Several numerical simulations (Mihos & Hernquist 1996; Di Matteo et al. 2005; Springel et al. 2005; Hopkins et al. 2006; DeBuhr et al. 2012) and observations (Alonso et al. 2007; Ellison et al. 2011; Sabater et al. 2013) have shown that the close pair interaction induces gas inflow into the galactic centre, enhancing both central SF and AGN activity, which is consistent with this finding.

Meanwhile, isolated galaxies experience less change in f_{AGN} and SFR_{fib} at a given ρ_{20} , but show an apparent change in the $L_{[\text{OIII}]}$. For example, for the most isolated galaxies

with the largest r_p at a given ρ_{20} , AGNs are not detected more frequently but the detected AGNs tend to be more luminous.

The most dramatic features are found in the cluster environment of $\rho_{20} > 20\bar{\rho}$, as shown in Figures 4 and 5. The f_{AGN} of galaxies with $r_p < 0.5r_{\text{vir,nei}}$ decreases as ρ_{20} increases and is the lowest at $\rho_{20} \sim 50\bar{\rho}$. On the other hand, despite the lowest SFR_{fib} , galaxies with $0.5r_{\text{vir,nei}} < r_p < 2r_{\text{vir,nei}}$ (i.e. cluster outskirts) show a significant excess of the AGN fraction when $\rho_{20} > 50\bar{\rho}$ (e.g. in rich clusters), but the level of AGN activity of them is weak.

3.3 Different environmental effects depending on central SFR

In this section, to examine the direct environmental effect on the nuclear activity of galaxies, we divide the high- σ sample into two subsamples according to the SFR_{fib} values as seen in Figure 1. The high- SFR_{fib} subsample consists of 670 galaxies, corresponding to about 22.8% of the high- σ sample. Table 2 lists the statistics of the full sample and subsamples we use.

3.3.1 Galaxies with high central star formation rate

This subsample of galaxies consists of SFGs and starburst-AGN composite hosts. In particular, in galaxies with a higher SFR_{fib} , higher luminosity composite hosts are found but the number is much smaller than that of SFGs. We examine the distributions of SFR_{fib} , f_{SFG} , and f_{AGN} of the sample in the r_p - ρ_{20} space.

The results are given in Figure 6. The high- SFR_{fib} galaxies are hardly found in rich clusters. On average, f_{SFG} is larger than f_{AGN} over the entire space. Table 2 shows that the AGNs hosted by the high- SFR_{fib} galaxies are more likely to be powerful.

The most notable feature is that over the entire space, the relation of an environment with f_{AGN} and f_{SFG} is opposite overall. We find that the SFGs are most often found in two specific environments where the starburst-AGN composite hosts are least found. One occupies a region of $r_p \gg r_{\text{vir,nei}}$ and $\rho_{20} \sim 10\bar{\rho}$ where galaxies are expected to have recently undergone a major merger in a rich group. The other occupies a region of $r_p < 0.3r_{\text{vir,nei}}$ and $7\bar{\rho} < \rho_{20} < 30\bar{\rho}$ which switches from group to cluster environment. Their f_{SFG} and f_{AGN} values are comparable to each other.

For the latter environment, the galaxies no longer exist in a very dense environment of $\rho_{20} > 40\bar{\rho}$. At $r_p < 0.3r_{\text{vir,nei}}$ and $\rho_{20} < 7\bar{\rho}$ (mostly groups), f_{SFG} and f_{AGN} change little but when ρ_{20} increases further, the values sensitively change, requiring that physical mechanisms in the clusters should be more effective than the galaxy interactions in the groups. As the system to which galaxies belong grows hierarchically, they are likely to experience a variety of physical mechanisms that funnel abundant gases to the centre. Meanwhile, their f_{SFG} and f_{AGN} values comparable to those of galaxies at late-stage of the gas-rich mergers in groups suggest that these galaxies may favour a merger-driven evolutionary scenario.

Figure 6 also shows that at those two locations, SFGs are found almost twice as many as AGN hosts. Although elsewhere, less SFGs are found and more AGN hosts are found. Interestingly, compared to the fractions in the two environments it seems that the decrease in f_{SFG} has led to the increase in f_{AGN} . The result indicates that the violent environments, possibly associated with merger events, cause a high gas accretion rate, not only inducing starbursts and rapid BH growth but also obscuring AGNs by dense gas and dust (see Hickox & Alexander 2018, for a review). On the other hand, other environments provide a moderate gas accretion rate, reducing f_{SFG} and more AGNs becomes observable. In a field environment where galaxies do not belong to a group or cluster, the lowest f_{SFG} and the highest f_{AGN} are found.

These interesting features associated with starburst-

AGN connection are unveiled only after excluding the low- SFR_{fib} galaxies (77% of the whole sample). This high- SFR_{fib} sample also demonstrates that an environment controls a gas accretion rate, eventually controlling a central SF and an obscuring medium nearby AGNs that intercepts AGN luminosity. Consequently, it is difficult to observe the direct impact of the environment with this gas-rich sample.

3.3.2 Galaxies with low central star formation rate

In this section, we examine the distributions in r_p - ρ_{20} space for SFR_{fib} , f_{AGN} and $u-r$ colour of the low- SFR_{fib} sample. The results are shown in Figure 7.

Since this SFR_{fib} -limited subsample has slightly different SFR_{fib} values, the SFR_{fib} distribution slightly depends on r_p and ρ_{20} . Therefore, it is not easy to estimate the r_p or ρ_{20} dependence of f_{AGN} at a given SFR_{fib} by comparing the left and middle panels of Figure 7. Therefore, we plot Figure 8 showing how f_{AGN} and SFR_{fib} vary depending on ρ_{20} at a given r_p . We investigate three different r_p cases: isolated galaxies ($r_p \sim 4.3r_{\text{vir,nei}}$), galaxies just entering the nearest neighbour's virial radius ($r_p \sim 1.5r_{\text{vir,nei}}$), and close-interacting galaxies ($r_p \sim 0.3r_{\text{vir,nei}}$) are examined separately. Each circle represents the median values for the galaxies at a fixed ρ_{20} . The error bars are calculated as bootstrapping errors using the bootstrapping method with 1000 runs.

Overall, galaxies in this subsample have low SFR_{fib} , low AGN power, and red colour. For the isolated galaxy case, SFR_{fib} in groups slightly depends on ρ_{20} and f_{AGN} changes little. They are almost free from the influence of the neighbours and background galaxies. Their SFR_{fib} - f_{AGN} relation is used as a control and for comparison, is drawn with a red line in each panel.

Figure 7 shows that the low- SFR_{fib} sample nearly retains the diverse environmental dependences of f_{AGN} seen in the whole SFR_{fib} sample, particularly at $r_p < r_{\text{vir,nei}}$. At $\rho_{20} < 10\bar{\rho}$ (i.e. groups), f_{AGN} is mostly sensitive to r_p . The f_{AGN} rapidly increases at $r_p < 0.3r_{\text{vir,nei}}$ while SFR_{fib} changes little at $r_p < 0.3r_{\text{vir,nei}}$, implying that at a given SFR_{fib} , close neighbour interactions in groups are significantly effective in enhancing f_{AGN} .

Meanwhile, the relation between f_{AGN} and SFR_{fib} in clusters becomes complex, completely different from that in groups. At $\rho_{20} \sim 50\bar{\rho}$ where f_{AGN} has the lowest value, as r_p decreases, f_{AGN} decreases but SFR_{fib} rather increases. This trend is also seen in the whole sample (see Figs. 4 and 5). As a galaxy moves within its cluster, a mechanism such as ram-pressure becomes dominant (Gunn & Gott 1972), likely compressing the gas into dense clouds, increasing SFR_{fib} but not f_{AGN} .

At $r_p \sim 0.3r_{\text{vir,nei}}$, f_{AGN} significantly decreases as a galaxy joins more and more rich systems while SFR_{fib} weakly decreases. Figure 7 also shows that galaxies belonging to the outer region of rich clusters show an f_{AGN} enhancement, although they have the lowest SFR_{fib} and the reddest $u-r$ colour. The green and red dots in the middle panel of Figure 8 show that the result is systematically significant although the errors are large. The reddest $u-r$ colour in the outer region of massive clusters implies that SF quenching has been already pre-processed. Despite the lowest SFR_{fib} in the outskirts of rich clusters, the strong enhancement in f_{AGN} requires a violent mechanism. Martini (2009) found

Table 2. Sample statistics

Number (Fraction)	Total	AGNs	^a Strong AGNs
All ($\sigma > 70 \text{ km s}^{-1}$)	11 096 (1.00)	2942 (0.27)	765 (0.07)
All ($130 \text{ km s}^{-1} < \sigma < 200 \text{ km s}^{-1}$)	2935 (1.00)	1079 (0.37)	400 (0.14)
High SFR _{fib} sample	670 (1.00)	231 (0.35)	158 (0.24)
Low SFR _{fib} sample	2265 (1.00)	848 (0.38)	242 (0.11)

Note: ^a Galaxies hosting a luminous AGN with $L_{[\text{OIII}]}$ $> 10^{40} \text{ erg s}^{-1}$.

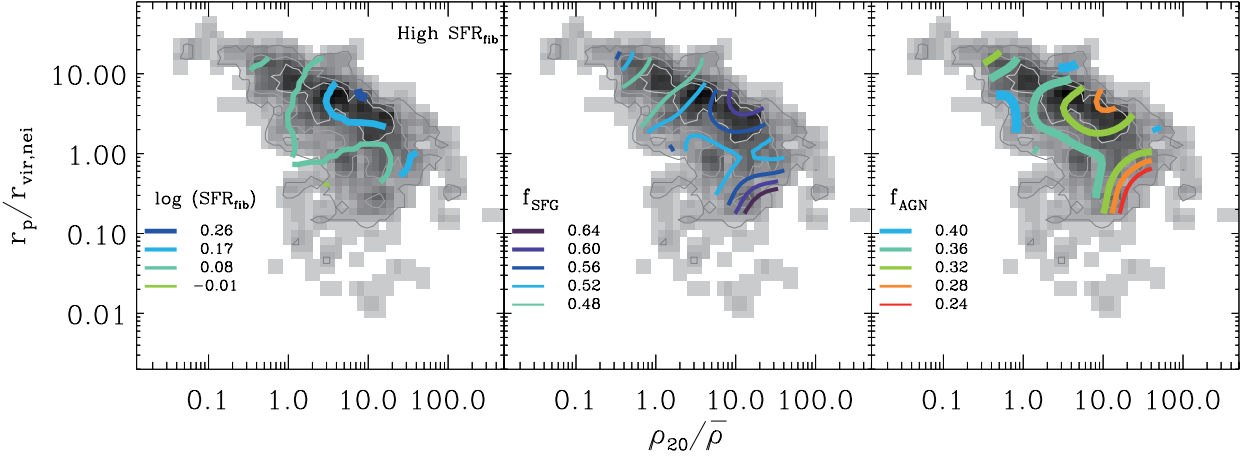


Figure 6. Distributions in the r_p – ρ_{20} plane of $\log(\text{SFR}_{\text{fib}})$ (left), f_{SFG} (middle), and f_{AGN} (right) of the high-SFR_{fib} galaxy sample. For the $\log(\text{SFR}_{\text{fib}})$ distribution, contours with a standard error of 1000 bootstrap estimates greater than 0.08 are eliminated. The grey 2D histogram and the grey thin contours represent the number density distributions of the sample.

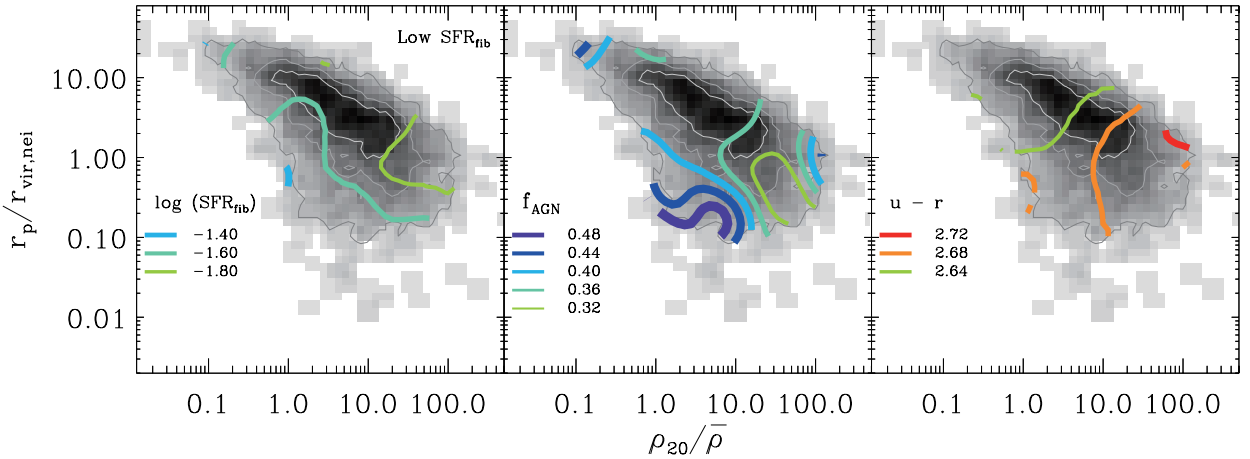


Figure 7. Distributions in the r_p – ρ_{20} plane of $\log(\text{SFR}_{\text{fib}})$ (left), f_{AGN} (middle), and $u-r$ colour (right) of the low-SFR_{fib} galaxy sample. The grey 2D histogram and the grey thin contours show the number density distributions of the sample. For the $\log(\text{SFR}_{\text{fib}})$ and $u-r$ distributions, contours with a standard error of 1000 bootstrap estimates greater than 0.1 and 0.02 are eliminated, respectively.

substantial numbers of AGNs on radial orbits in clusters and argued that they recently entered the clusters. Some studies found that the AGN fractions of spiral galaxies at outer cluster radii are as large as those of field galaxies (Haggard et al. 2010; Hwang et al. 2012; Sohn et al. 2013).

4 DISCUSSION

4.1 High central SF and obscured AGN: the starburst-AGN connection

In general, if the gas causing starburst is also responsible for feeding the AGN, then a positive correlation is expected. However, we identified galaxies with a negative correlation (high SFR_{fib} but low f_{AGN}) in two specific environments.

The r_p – ρ_{20} diagram allows us to deduce what mech-

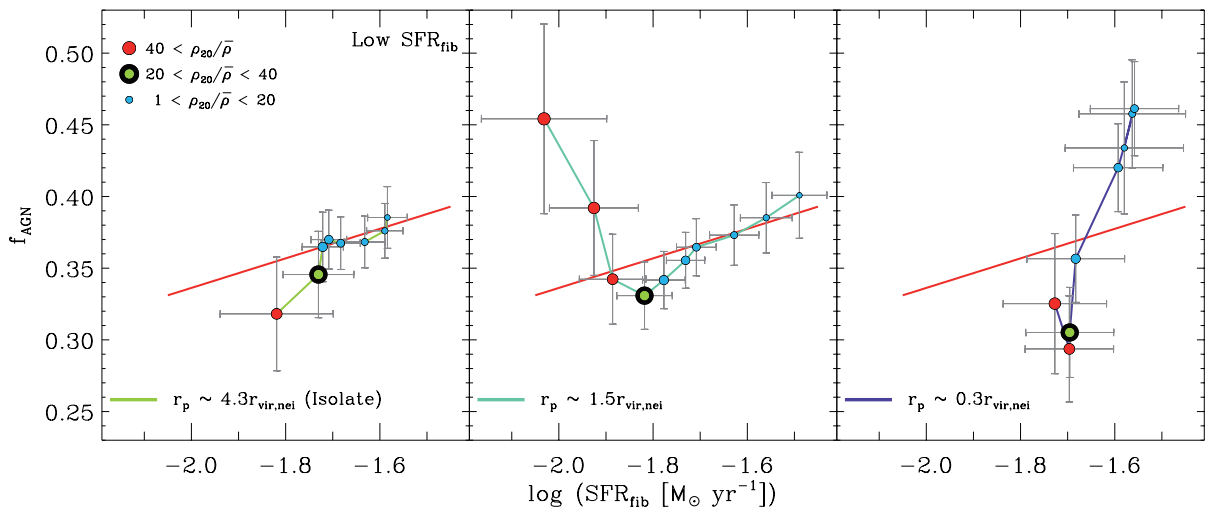


Figure 8. The ρ_{20} dependency of SFR_{fib} and f_{AGN} at given r_p for the low- SFR_{fib} sample. Three cases with different r_p values are investigated: (left) isolated galaxies ($r_p \sim 4.3r_{\text{vir,nei}}$), (middle) galaxies just about to enter their nearest neighbour’s virial radius ($r_p \sim 1.5r_{\text{vir,nei}}$), and (right) galaxies in close interaction ($r_p \sim 0.3r_{\text{vir,nei}}$). The size of bins used to fix the r_p and ρ_{20} values of the sample is $\Delta(\log r_p/r_{\text{vir,nei}}) = 0.23$ and $\Delta(\log \rho_{20}/\bar{\rho}) = 0.23$, respectively. The colour and size of the dots change depending on ρ_{20} . The errors represent $1\text{-}\sigma$ deviation from 1000 bootstrap resampling. For comparison, the relation between SFR_{fib} and f_{AGN} of the isolated galaxies is drawn in each panel with a red line.

anisms cause large quantities of gas to inflow into the central regions, leading to rapid SF quenching. In the region of $r_p \gg r_{\text{vir,nei}}$ and the intermediate- ρ_{20} s, the lowest f_{AGN} and the highest f_{SFG} are found. The AGNs observed at this stage (i.e. starburst-AGN composite) are small in number but have high luminosity. We infer that they are at late-stage of the gas-rich mergers inducing high accretion rates (e.g., Park & Choi 2009), which is in agreement with the observation that the most luminous AGNs require major mergers (Treister et al. 2012). Here, we speculate that surrounded by dense gases and dust, AGNs are hidden in SFGs (particularly, massive ones), leading to the lowest f_{AGN} . Barnes & Hernquist (1991) suggested in a simulation that violent tidal forces occurred during a gas-rich galaxy merger trigger the bar formation supplying the gas fuel to a BH and a violent SF in central gas clouds is accompanied. Indeed, infrared and hard X-ray-selected AGNs less sensitive to obscuration by gas and dust have apparent connections to galaxy mergers (e.g., Veilleux et al. 2009; Koss et al. 2010; Satyapal et al. 2014; Kocevski et al. 2015; Ricci et al. 2017). Satyapal et al. (2014) found by using cross-matched SDSS and Wide-field Infrared Survey Explorer (WISE) data that galaxies in late-stage mergers show a higher excess of IR-selected AGNs than optically selected AGNs, even in post-merger galaxies sample.

Surprisingly, the starburst-AGN connection-related feature is found even in a dense environment. As a gas-rich galaxy moves within clusters, repeated high-speed encounters (or weak encounters, Moore et al. 1998) or tids in clusters can disturb galaxies or direct gas inflow towards the central region, thus enhancing SFR_{fib} and triggering a lot of AGNs. The interaction between galaxy and hot intra-cluster medium (ICM) directly can also affect AGN activity of cluster galaxies. For example, the ram-pressure stripping in clusters can also compress the galaxy interstellar medium, which also enhances the SFR (e.g., Fujita & Nagashima 1999). Kronberger et al. (2008) found in simulated spiral galaxies

that the SF enhancement can take place in the central part of galaxies, where the interstellar medium is compressed by the ram-pressure of the surrounding ICM. Bekki & Couch (2003, 2011) also demonstrated that ram-pressure induces the collapse of molecular clouds and consequently trigger a starburst. Poggianti et al. (2017) have discovered a causal connection between ram-pressure stripping and AGN activity from a jellyfish galaxy in clusters. In contrast, the ram pressure at the centre of rich clusters removes a significant amount of cold gas within a galaxy, leading to SF quenching.

As an alternative, the group-cluster merger is possible. Gas-rich galaxies in in-falling group may experience mergers and strong encounters in the in-fall region of the cluster (e.g., Vijayaraghavan & Ricker 2013). Hwang et al. (2018) showed in numerical simulation that while spiral galaxies fall into the cluster environment, galaxy–galaxy multiple interactions at high-speed enhance SF activity in spiral galaxies. Jaffé et al. (2016) also showed that gas-rich galaxies are found in the recent in-fall region of the cluster or even inside the cluster.

In these violent environments, some of these may undergo a morphological transformation into gas-poor S0 galaxies (e.g. D’Onofrio et al. 2015). Unfortunately, we could not see perturbed signatures in the SFGs due to the spatial resolution of the SDSS imaging. Along with these results, the reduction in f_{SFG} and the enhancement in f_{AGN} measured in other relatively mild environments indicate that an environment affects a gas accretion rate, contributing to SF quenching and AGN detection, particularly for gas-rich galaxies.

4.2 Enhanced AGN fraction in cluster environments

The most dramatic environmental impact is found in quiescent spiral galaxies with relatively large pair separations ($0.5r_{\text{vir,nei}} < r_p < 2r_{\text{vir,nei}}$) in the very high-density region

of $\rho_{20} > 50\bar{\rho}$. It is estimated that they are in the outskirts of rich clusters. They have a higher f_{AGN} than in cluster centres and the AGNs have low luminosity. They also have rather redder colour and lower SFR_{fib} even when compared to galaxies inside the clusters, suggesting that they have already experienced a ‘sudden’ SF quenching mechanism.

Galaxy starvation (Larson et al. 1980) occurs on the cluster outskirts but is not suitable for the rapid SF quenching. Once galaxies enter the cluster, in the beginning, tidal effects via the large gravitational potential of clusters can cause hot gas to escape within a galaxy, but not cold gas. Accordingly, the cold gas is gently removed through SF. In contrast, ram-pressure stripping can remove a significant amount of cold gas within a galaxy, resulting in quenching. However, it requires a dense ICM and a high relative velocity of a galaxy to the ICM, which is dominant at the centre of rich clusters.

Meanwhile, according to the hierarchical structure formation paradigm, clusters grow via the in-fall of galaxies (in groups) along the filaments surrounding a cluster. McGee et al. (2009) and De Lucia et al. (2012) argued that about 40 ~ 50% of galaxies in massive clusters has arrived as members of in-falling groups and the in-falling group galaxies could already be subjected to ‘pre-processing’ in group environments, prior to entering the cluster. Fassbender et al. (2012) argued that galaxies with relatively lower velocity dispersions than those of central cluster galaxies may result from the in-falling groups, thus raising the galaxy merger rate. Koulouridis & Bartalucci (2019) suggested galaxy mergers as a dominant mechanism of the X-ray-detected AGN excess found in the outskirts of massive clusters at $z \sim 1$. Vazza et al. (2011) also demonstrated a high merger rate in the outskirts of massive clusters by using high-resolution cosmological simulations.

Meanwhile, cluster galaxies with $r_p < 0.3r_{\text{vir,nei}}$ at $\rho_{20} \sim 40\bar{\rho}$ may move faster in the inner regions of clusters where mergers and interaction become less frequent and most encounters occur as high-speed fly-bys. Due to the strong ram-pressure stripping, they may contain only very little cold gas. For the non-merging quiescent case, the stochastic accretion through secular processes becomes dominant and drives less luminous AGN activity (see Hopkins et al. 2014). Indeed, our result shows that they have the lowest f_{AGN} in the r_p - ρ_{20} space and the AGNs appear to be less luminous.

5 SUMMARY

We identified 1 079 Type II AGNs (36.8%) in a volume- and σ -limited sample of 2,935 spiral galaxies with $0.02 < z < 0.055$, $M_r < -19.5$, and $130 \text{ km s}^{-1} < \sigma < 200 \text{ km s}^{-1}$, selected from SDSS DR7, to determine a direct environmental effects on AGN activity. To define the environmental measurements, we used a volume-limited sample with $0.02 < z < 0.055$ and $M_r < -19.0$. The combined impacts of the large-scale background density and interactions with the most influential neighbour are investigated. Since the environment can affect both the central SF and AGN activity, the central SFR_{fib} of the sample is additionally limited to separate only the effect on AGN activity. Two subsamples of before and after AGN peak in the SFR_{fib} - σ diagram are used.

Our primary results are summarized as follows:

(i) The AGN fraction is related to the central SFR depending on the availability of central gas fuels.

At a given σ , galaxies with very high central SFRs have the lowest AGN fraction, but the luminosity of the detected AGNs is the highest. As the central SFR considerably decreases, the AGN fraction reaches its peak. The luminosity of the AGNs at the peak is already significantly reduced. The result shows that the central SFR and AGN luminosity (BH accretion rate) are closely related.

(ii) Galaxies with the highest SFR_{fib} but the lowest f_{AGN} are found in two violent environments of groups and (poor) clusters. We argue here that the low f_{AGN} value is due to the difficulty in observing triggered AGNs in this optical survey rather than the difficulty in inducing AGN activity itself and that according the starburst-AGN connection, the SFGs optically obscured AGNs.

Indeed, they are found in rich groups where recent merger products are often found and in clusters where the combined effect of ram pressure and frequent weak encounters dominates. Considering the merger-AGN connection, the latter galaxies may also be greatly affected by a hierarchical merger that occurs during system growth from group to cluster.

These gas-rich galaxies with massive bulge clearly shows that an environment controls a gas accretion rate, eventually controlling a central SF and an obscuring medium nearby AGNs that intercepts AGN luminosity.

(iii) The observational evidence of the direct environmental effect is clearly found in red spiral galaxies resided in the outskirts of rich clusters. They show a higher AGN fraction despite the lack of gas (indicated by the lowest SFR_{fib} and the reddest colour). This suggests that the SF quenching process has already completed and that a strong galaxy interaction or a galaxy merging that occurs in the cluster outskirts accelerate the accretion of remained surrounding matter onto a BH.

This study highlights how important mergers are in driving AGN activity and galaxy evolution. In particular, galaxy–galaxy mergers in group environments and group-cluster mergers in cluster outskirts clearly demonstrate AGN-galaxy co-evolution. Indeed, the role of galaxy mergers in fuelling AGN has often been debated. In particular, because the correlation between mergers and detected AGN fraction is highly sensitive to obscuration by gas and dust, optical surveys have not clarified this correlation. Although we use optically selected AGNs found in the local Universe, by considering a volume-limited spiral galaxy sample according to central velocity dispersion and central SFR, we yield observational evidence with high reliability regarding the impact of merger processes on AGN triggering depending on the local background galaxy density. The use of such a large data set has led to a detailed and robust statistical description of the environmental dependence of AGN activity.

ACKNOWLEDGEMENTS

We thank the anonymous referee for useful and detailed comments that improved significantly the original manuscript.

We acknowledge support from the National Research

Foundation (NRF) of Korea to the Center for Galaxy Evolution Research (No. 2017R1A5A1070354). The work by SSK was supported by the NRF grant funded by the Ministry of Science and ICT of Korea (NRF-2014R1A2A1A11052367). This work was also supported by the BK21 plus program through the NRF funded by the Ministry of Education of Korea.

Funding for the SDSS and SDSS-II has been provided by the Alfred P. Sloan Foundation, the Participating Institutions, the National Science Foundation, the U.S. Department of Energy, the National Aeronautics and Space Administration, the Japanese Monbukagakusho, the Max Planck Society, and the Higher Education Funding Council for England. The SDSS Web site is <http://www.sdss.org/>. The SDSS is managed by the Astrophysical Research Consortium for the Participating Institutions. The Participating Institutions are the American Museum of Natural History, Astrophysical Institute Potsdam, University of Basel, Cambridge University, Case Western Reserve University, University of Chicago, Drexel University, Fermilab, the Institute for Advanced Study, the Japan Participation Group, Johns Hopkins University, the Joint Institute for Nuclear Astrophysics, the Kavli Institute for Particle Astrophysics and Cosmology, the Korean Scientist Group, the Chinese Academy of Sciences (LAMOST), Los Alamos National Laboratory, the Max-Planck-Institute for Astronomy (MPIA), the Max-Planck-Institute for Astrophysics (MPA), New Mexico State University, Ohio State University, University of Pittsburgh, University of Portsmouth, Princeton University, the United States Naval Observatory, and the University of Washington.

REFERENCES

- Abazajian, K. N., et al., 2009, *ApJS*, 182, 543
Aird, J., et al., 2012, *ApJ*, 746, 90
Alexander, D. M., & Hickox, R. C., 2012, *New Astron. Rev.*, 56, 93
Alonso, M. S., Lambas, D. G., Tissera, P., & Coldwell, G., 2007, *MNRAS*, 375, 1017
Alonso, M. S., Coldwell, G., & Lambas, D. G., 2013, *A&A*, 549, A141
Argudo-Fernández, M., Shen, S., Sabater, J., Duarte Puertas, S., Verley, S., Yang, X., 2016, *A&A*, 592, A30
Argudo-Fernández, M., Lacerna, I., & Duarte Puertas, S., 2018, *A&A*, 620, A113
Baldwin, J. A., Phillips, M. M., & Terlevich, R., 1981, *PASP*, 93, 5
Banerjee, P., Szabo, T., Pierpaoli, E., Franco, G., Ortiz, M., Ormas, A., Tornello, B., 2018, *New Astron.*, 58, 61
Barnes, J. E., Hernquist, L. E., 1991, *ApJ*, 370, L65
Batiste, M., Bentz, M. C., Raimundo, S. I., Vestergaard, M., & Onken, C. A., 2017, *ApJ*, 838, L10
Bekki, K., & Couch, W. J., 2003, *ApJ*, 596, L13
Bekki, K., & Couch, W. J., 2011, *MNRAS*, 415, 1783
Bernardi, M., et al., 2003, *AJ*, 125, 1817
Blanton, M. R., et al., 2005, *AJ*, 129, 2562
Brinchmann, J., Charlot, S., White, S. D. M., Tremonti, C., Kauffmann, G., Heckman, T., Brinkmann, J., 2004, *MNRAS*, 351, 1151
Chang, Y.-Y., et al., 2017, *ApJS*, 233, 19
Cheung, E., et al., 2015, *ApJ*, 807, 36
Choi, Y.-Y., Woo, J.-H., & Park, C., 2009, *ApJ*, 699, 1679
Choi, Y.-Y., Han, D.-H., & Kim, S. S., 2010, *J. Korean Astron. Soc.*, 43, 191
Cid Fernandes, R., et al., 2010, *MNRAS*, 403, 1036
Cid Fernandes, R., Stasińska, G., Mateus, A., & Vale Asari, N., 2011, *MNRAS*, 413, 1687
Ciotti, L., & Ostriker, J. P., 2007, *ApJ*, 665, 1038
Combes, F., 2003, in Collin S., Combes F., Shlosman I., eds, *ASP Conf. Ser. Vol. 290, Active Galactic Nuclei: From Central Engine to Host Galaxy*, Astron. Soc. Pac., San Francisco, p. 411
D’Onofrio, M., Marziani, P., & Buson, L., 2015, *Front. Astron. Space Sci.*, 2, 4
Darg, D. W., et al., 2010, *MNRAS*, 401, 1552
Davies, R., Burtscher, L., Dodds-Eden, K., & Orban de Xivry, G., 2012, *J. Phys. Conf. Ser.* 372, 012046
DeBuhr, J., Quataert, E., & Ma, C.-P., 2012, *MNRAS*, 420, 2221
De Lucia, G., Weinmann, S., Poggianti, B. M., Aragón-Salamanca, A., & Zaritsky, D., 2012, *MNRAS*, 423, 1277
Di Matteo, T., Springel, V., & Hernquist, L., 2005, *Nature*, 433, 604
Ellison, S. L., Patton, D. R., Mendel, J. T., & Scudder, J. M., 2011, *MNRAS*, 418, 2043
Elmegreen, B. G., et al., 1998, *ApJ*, 503, L119
Fassbender, R., Šuhada, R., & Nastasi, A., 2012, *Adv. Astron.*, 2012, 138380
Ferrarese, L., & Merritt, D., 2000, *ApJ*, 539, L9
Fisher, D. B., & Drory, N., 2010, *ApJ*, 716, 942
Fujita, Y., Nagashima, M., 1999, *ApJ*, 516, 619
Gebhardt, K., et al., 2000, *ApJ*, 539, L13
Goulding, A. D., et al., 2018, *PASJ*, 70, S37
Grogin, N. A., et al., 2005, *ApJ*, 627, L97
Gültekin, K., et al., 2009, *ApJ*, 698, 198
Gunn, J. E., & Gott, J. R., 1972, *ApJ*, 176, 1
Haan, S., Schinnerer, E., Emsellem, E., Garcia-Burillo, S., Combes, F., Mundell, C. G., Rix, H.-W., 2009, *ApJ*, 692, 1623
Haggard, D., Green, P. J., Anderson, S. F., Constantin, A., Aldcroft, T. L., Kim, D.-W., Barkhouse, W. A., 2010, *ApJ*, 723, 1447
Hernquist, L., & Mihos, J. C., 1995, *ApJ*, 448, 41
Hickox, R. C., & Alexander, D. M., 2018, *ARA&A*, 56, 625
Hopkins P. F., Hernquist L., Cox T. J., Di Matteo, T., Martini, P., Robertson, B., Springel, V., 2005, *ApJ*, 630, 705
Hopkins, P. F., Hernquist, L., & Cox, T. J., 2006, *ApJS*, 163, 1
Hopkins, P. F., Hernquist, L., Cox, T. J., & Kereš, D., 2008, *ApJS*, 175, 356
Hopkins, P. F., Kocevski, D. D., & Bundy, K., 2014, *MNRAS*, 445, 823
Hwang, H. S., Park, C., Elbaz, D., & Choi, Y.-Y., 2012, *A&A*, 538, A15
Hwang, J.-S., Park, C., Banerjee, A., & Hwang, H. S., 2018, *ApJ*, 856, 160
Ishibashi, W., & Fabian, A. C., 2016, *MNRAS*, 463, 1291
Jaffé, Y. L. et al., 2016, *MNRAS*, 461, 1202
Kauffmann, G., et al., 2003, *MNRAS*, 346, 1055
Kauffmann, G., et al., 2007, *ApJS*, 173, 357
Kewley, L. J., Dopita, M. A., Sutherland, R. S., Heisler, C. A., & Trevena, J., 2001, *ApJ*, 556, 121
Kewley, L. J., Groves, B., Kauffmann, G., & Heckman, T., 2006, *MNRAS*, 372, 961
Kim, M., Choi, Y.-Y., & Kim, S. S., *MNRAS*, in submitted
Kocevski D. D., et al., 2015, *ApJ*, 814, 104
Kormendy, J., & Kennicutt, Jr. R. C., 2004, *ARA&A*, 42, 603
Koss M., Mushotzky R., Veilleux S., Winter L., 2010, *ApJL*, 716, L125
Koulouridis, E., & Bartalucci, I., 2019, *A&A*, 623, L10
Kronberger T., Kapferer W., Ferrari C., Unterguggenberger S., & Schindler, S., 2008, *A&A*, 481, 337
LaMassa, S. M., Heckman, T. M., Ptak, A., & Urry, C. M., 2013, *ApJ*, 765, L33

- Larson, R. B., Tinsley, B. M., & Caldwell, C. N., 1980, *ApJ*, 237, 692
- Liu, X., Shen, Y., & Strauss, M. A. 2012, *ApJ*, 745, 94
- Lynden-Bell, D., 1969, *Nature*, 223, 690
- Martini, P., Sivakoff, G. R., & Mulchaey, J. S., 2009, *ApJ*, 701, 66
- McConnachie, A. W., Patton, D. R., Ellison, S. L., & Simard, L., 2009, *MNRAS*, 395, 255
- McGee, S. L., Balogh, M. L., Bower, R. G., Font, A. S., & McCarthy, I. G., 2009, *MNRAS*, 400, 937
- Melnick, J., & De Propriis, R., 2013, *MNRAS*, 431, 2034
- Mihos, J. C., & Hernquist, L., 1996, *ApJ*, 464, 641
- Moles, M., Márquez, I., & Pérez, E., 1995, *ApJ*, 438, 604
- Monaghan, J. J., & Lattanzio, J. C. 1985, *A&A*, 149, 135
- Moore, B., Lake, G., & Katz, N., 1998, *ApJ*, 495, 139
- Park, C., & Choi, Y.-Y., 2005, *ApJ*, 635, L29
- Park, C., Choi, Y.-Y., Vogeley, M. S., Gott, J. R. III, Blanton, M. R., SDSS Collaboration, 2007, *ApJ*, 658, 898
- Park, C., Gott, J. R., & Choi, Y. Y., 2008, *ApJ*, 674, 784
- Park, C., & Choi, Y.-Y., 2009, *ApJ*, 691, 1828
- Poggianti, B. M., Jaffé, Y. L., Moretti, A., et al., 2017, *Nature*, 548, 304
- Rees, M. J., 1984, *ARA&A*, 22, 471
- Ricci C., et al., 2017, *MNRAS*, 468, 1273
- Sabater, J., Verdes-Montenegro, L., Leon, S., Best, P., & Sulentic, J., 2012, *A&A*, 545, A15
- Sabater, J., Best, P. N., & Argudo-Fernández, M., 2013, *MNRAS*, 430, 638
- Sabater, J., Best, P. N., & Heckman, T. M., 2015, *MNRAS*, 447, 110
- Salim, S., et al., 2007, *ApJS*, 173, 267
- Sanders, D. B., Soifer, B. T., Elias, J. H., Madore, B. F., Matthews, K., Neugebauer, G., Scoville, N. z., 1988, *ApJ*, 325, 74
- Satyapal, S., Ellison, S. L., McAlpine, W., Hickox, R. C., Patton, D. R., Mendel, J. T., 2014, *MNRAS*, 441, 1297
- Schawinski, K., et al., 2010, *ApJ*, 711, 284
- Scott, C., & Kaviraj, S., 2014, *MNRAS*, 437, 2137
- Serra, A. L., & Diaferio, A., 2013, *ApJ*, 768, 116
- Shlosman, I., Begelman, M. C., & Frank, J., 1990, *Nature*, 345, 679
- Slavcheva-Mihova, L., & Mihov, B., 2011, *A&A*, 526, A43
- Sohn, J., Hwang, H. S., Lee, M. G., Lee, G.-H., & Lee, J. C., 2013, *ApJ*, 771, 106
- Springel, V., Di Matteo, T., & Hernquist, L., 2005, *ApJ*, 620, L79
- Stasińska, G., et al., 2008, *MNRAS*, 391, L29
- Treister, E., Schawinski, K., Urry, C. M., & Simmons, B. D., 2012, *ApJL*, 758, L39
- Tremaine, S., et al., 2002, *ApJ*, 574, 740
- Vazza, F., Roncarelli, M., Ettori, S., & Dolag, K., 2011, *MNRAS*, 413, 2305
- Veilleux, S., & Osterbrock, D. E., 1987, *ApJS*, 63, 295
- Veilleux, S., et al., 2009, *ApJS*, 182, 628
- Vijayaraghavan, R., & Ricker, P. M. 2013, *MNRAS*, 435, 2713
- Villforth, C., et al., 2014, *MNRAS*, 439, 3342
- von der Linden, A., Wild, V., Kauffmann, G., White, S. D. M., & Weinmann, S., 2010, *MNRAS*, 404, 1231
- Wada, K., 2004, *Coevolution of Black Holes and Galaxies* ed. L. C. Ho (Cambridge: Cambridge Univ. Press), 186
- Wada, K., Papadopoulos, P. P., & Spaans, M., 2009, *ApJ*, 702, 63
- Weston, M. E., McIntosh, D. H., Brodwin, M., Mann, J., Cooper, A., McConnel, A., Nielsen, J. L., 2017, *MNRAS*, 464, 3882

This paper has been typeset from a $\text{\TeX}/\text{\LaTeX}$ file prepared by the author.